Kinetic Models for Coal Hydrogasification and Analyses of Hydrogasification Characteristics in Entrained-Flow Gasifiers

ARTICLE *in* ENERGY & FUELS · OCTOBER 2013

Impact Factor: 2.79 · DOI: 10.1021/ef401302b

6 AUTHORS, INCLUDING:

He Boshu
Beijing Jiaotong University
47 PUBLICATIONS **240** CITATIONS
SEE PROFILE

Zhipeng Duan
Beijing Jiaotong University
42 PUBLICATIONS **345** CITATIONS
SEE PROFILE

energy&fuels

Article

pubs.acs.org/EF

Kinetic Models for Coal Hydrogasification and Analyses of Hydrogasification Characteristics in Entrained-Flow Gasifiers

Linbo Yan, Boshu He,* Xiaohui Pei, Chaojun Wang, Xusheng Li, and Zhipeng Duan

School of Mechanical, Electronic and Control Engineering, Beijing Jiaotong University, Beijing 100044, People's Republic of China

ABSTRACT: Coal hydrogasification (CHG) is a promising technology for clean and efficient coal utilization. However, the kinetic mechanism of CHG has not been fully understood, and multidimensional numerical simulations of CHG in entrained-flow gasifiers are still rarely reported. To evaluate and optimize hydrogasification parameters in an entrained-flow-bed gasifier, it is necessary to develop a reasonable CHG kinetic model and carry out the corresponding numerical simulations. In this work, a CHG kinetic model, including five homogeneous reactions and three heterogeneous reactions, is established. Thereinto, for the heterogeneous reactions, a novel combined random pore and shrinking-core model with pressure correction (CRPSC−PC) is put forward to predict the char−gas reaction process. When the CHG model is set up, it is then loaded to the commercial computational fluid dynamics (CFD) package, Fluent, via the user-defined function (UDF), and the simulation results are validated against literature-available experimental data for entrained-flow coal hydrogasifiers. Good agreements between the simulation results and the experimental data are detected, which indicates that the model is reliable and can be used to predict the effects of different operating parameters on entrained-flow CHG. Finally, the CHG properties in the cylindrical entrained-flow gasifiers are analyzed on the basis of the experiments reported in the literature, and the CH_4 concentration in the gasification product is found to increase with the increasing H_2O concentration of the gasification agent, the increasing inlet temperature of the gasification agent when the H_2O concentration is high, and the increasing gasification pressure when the H_2 concentration is high.

1. INTRODUCTION

Coal is the most abundant but dirtiest fuel in the world.[1] Although traditional coal utilization technologies, such as coal direct combustion, have greatly boosted economic development, large quantities of pollutants have also been discharged into the environment concomitantly. Recently, with the advent of fears about climate change and energy crisis, more and more attention has been put on energy security and environmental sustainability.[2] Against this background, many technologies have been developed for clean and efficient coal utilization, and most of these technologies are based on coal gasification. One of these technologies, the zero emission coal (ZEC) system put forward by the Zero Emission Coal Alliance (ZECA) and developed by Los Alamos National Laboratory (LANL) is expected to reach an efficiency of about 70% with nearly zero amount of CO_2 and other pollutants discharge, and it is based on the coal hydrogasification (CHG) technology.[3−5] In fact, hydrogasification of coal has attracted more and more attention recently for its unique advantages. For example, the hydrogasification reaction is exothermic, and thus, no additional heat is required; the direct product of hydrogasification is methane; therefore, no additional methanator is required; the hydrogasification process has high thermal efficiency close to 80%; and there is no requirement for a catalyst.[6,7] Some lab-scale experiments have been performed by researchers around the world to study the effects of different operating conditions on CHG products and char reactivity.[8−10] In addition, some semi-industrial hydrogasifiers have also been developed by some institutes, such as Cities Service, Rocketdyne, Pittsburgh Energy Research Center, and Brookhaven National Laboratory.[11−13] The development of mathematic models about CHG, however, lags relatively behind the applications, although some kinetic models about coal gasification with steam and/or oxygen have been reported in the literature,[14,15] which is unfavorable for the evaluation and optimization of coal hydrogasifiers. Blackwood et al.[16,17] once proposed that coal hydrogenation was a two-stage process. The first stage was the fast hydrogenation of volatile constituents, and the second stage was the relatively slow char hydrogenation. They developed a correlation to calculate the apparent reaction rate of char hydrogasification, and the kinetic parameters were obtained from experiments. Their work is valuable for the following researchers. However, the kinetic parameters were mainly based on a fixed coal bed, and the diffusion effects did not appear in the correlation. Wen et al.[18] once developed an empirical correlation to calculate the rate of char hydrogenation. The model correlated the rate of hydrogasification with the hydrogen partial pressure and the amount of char left. The major shortcoming of this model is the necessity to know the amount of potential rapid-rate carbon as a function of the pertinent parameters.[19] Moseley et al.[20] proposed that thermal decomposition of coal produces not only volatiles but also active sites that form either methane by hydrogenation or unreactive char by cross-linking and gave a correlation similar to that presented by Wen. On the basis of the work performed by Wen and Paterson, some similar correlations were also developed by the following researchers.[19] Tomeczek et al.[21] once developed a kinetic model for char hydrogasification using the active center theory based on experimental data obtained from a fixed-bed hydrogasifier.

Received: July 10, 2013
Revised: October 16, 2013
Published: October 17, 2013

   dx.doi.org/10.1021/ef401302b | *Energy Fuels* 2013, 27, 6388−6396

All of the above models focus only on the mechanism of the coal (char) hydrogenation reaction and are not sufficient to reflect the whole hydrogasification process because many other reactions also take place simultaneously during the hydrogasification. The Institute of Gas Technology (IGT) once developed a CHG kinetic model,[22,23] which can properly predict the hydropyrolysis and hydrogasification processes. However, the model used uncommon coal composition analysis, and it cannot predict precisely the evolution of an individual species. Moreover, only C, H, and O elements are considered, and it is not the real case of coal. Besides the lagging of the CHG mechanisms, multidimensional numerical simulation about CHG has not yet been seen, which is also adverse to the development of CHG technology. In comparison to the previous work, three meaningful and original things about CHG are performed in this work. First, a relatively complete CHG kinetic model, including five homogeneous reactions and three heterogeneous reactions, is established to predict the CHG characteristics. A common coal analysis method is used in the present model, and the evolution of individual species can be predicted. Second, it is known that the mechanism of the heterogeneous reactions is complex and sometimes even uncertain. A reliable model should consider as fully as possible the factors that can affect the gas−char heterogeneous reactions. To better reflect the char−gas heterogeneous reaction process, a combined random pore and shrinking-core model with pressure correction (CRPSC−PC) is developed. Third, when the CHG model is set up, it is then programmed and loaded to the commercial computational fluid dynamics (CFD) package, Fluent, via the user-defined function (UDF), and the simulation results found agree well with the corresponding literature available experimental data, which implies that the CHG kinetic model developed in this work is reliable and can be used to predict the operation behavior of entrained-flow-bed CHG. Thus, the simulation of the CHG process in entrained-flow gasifiers can be very flexible, which is beneficial to the development of the CHG technology. Finally, the CHG properties in the cylindrical entrained-flow gasifiers are analyzed on the basis of the experiments reported in the literature rather than the simulations because there has been abundant experimental data reported for the cylindrical reactors. In our following research,a gasifier is expected to be found that can be potentially used in the ZEC system. The operation conditions will be designed, and the model setup in this work will be used for the evaluation and optimization of that gasifier.

2. HYDROGASIFICATION MODELS

In the present CHG kinetic model, the processes of pyrolysis, volatile homogeneous reactions, and char−gas heterogeneous reactions are all included. Coal is typically composed of five elements, including C, H, O, N, and S. The gaseous species in the model include H_2, CO, CO_2, CH_4, C_2H_6, C_6H_6, H_2O, H_2S, and SO_2. Char is considered to be solid carbon [C(s)]. The schematic diagram of the kinetic model developed in this work is shown in Figure 1. The entire CHG process is controlled by five homogeneous reactions and three heterogeneous reactions. The mechanisms of the gaseous homogeneous reactions are conventional and can be obtained from the literature, while those of the char−gas heterogeneous reactions are, however, much more complex because of the random particle shape and the complex reaction process, including the reactant diffusion, adsorption, surface reaction, desorption, and product diffusion. Thus, the calculation of the heterogeneous reactions must be carefully treated. In this work, a novel CRPSC−PC model is developed to reflect the char−gas heterogeneous reactions. It should be noted that, in Fluent, volatile

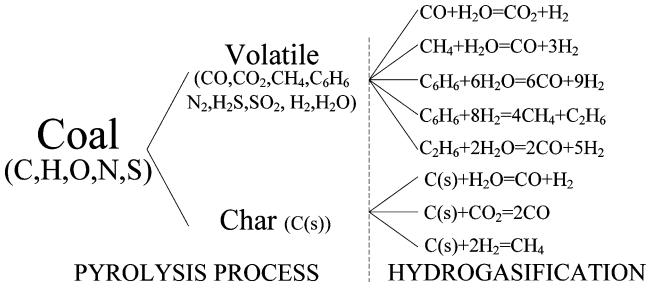

Figure 1. Schematic diagram of the CHG kinetic model.

from coal is treated as an integrated combustible, which cannot be used directly in the model developed in this work. To model individual species reactions, the volatile is managed as decomposing into H_2, CO, CO_2, CH_4, C_6H_6, H_2O, H_2S, and SO_2 rapidly based on species mass balance.

2.1. Coal Pyrolysis Model. Coal devolatilization can be modeled with the two competing rates model,[24] which has been widely practiced and accepted in engineering and can be expressed as eqs 1 and 2

$$\mathcal{R}_1 = A_1 e^{-(E_1/RT_p)} \tag{1}$$

$$\mathcal{R}_2 = A_2 e^{-(E_2/RT_p)} \tag{2}$$

where $\mathcal{R}_1$ and $\mathcal{R}_2$ are the competing rates that may control the devolatilization over different temperature ranges. The two kinetic rates are weighted to yield an expression for the devolatilization as eq 3

$$\frac{m_v(t)}{(1-f_{w,0})m_{p,0} - m_a} = \int_0^t (\alpha_1\mathcal{R}_1 + \alpha_2\mathcal{R}_2)\exp(-\int_0^t (\mathcal{R}_1 + \mathcal{R}_2)\mathrm{d}t)\mathrm{d}t \tag{3}$$

where $m_v(t)$ is the volatile yield up to time t, $f_{w,0}$ is the mass fraction of evaporating/boiling material, $m_{p,0}$ is the initial particle mass at injection, m_a is the ash content in the particle, and α_1 and α_2 are the yield factors.

2.2. Homogeneous Reactions. Five gaseous reactions listed in Table 1 are considered in this CHG kinetic model besides the volatile rapid endothermic decomposition reaction, R1. The stoichiometric number, a_i, is calculated on the basis of the species mass balance. R2 is the water−gas shift reaction, which will affect the volume fractions of CO, H_2O, CO_2, and H_2 in the gasification product. R3 is the methane reformation reaction, which reflects the interconversion of CH_4 and H_2. In this work, the pyrolysis product, tar, is assumed to be C_6H_6;[25] therefore, the reformation and hydrogenation reactions of C_6H_6 are considered as shown by R4 and R5. Although the amount of C_2H_6 is relatively small, the corresponding reformation reaction is considered with R6.

$$\text{volatile} \rightarrow a_1\text{CO} + a_2\text{CO}_2 + a_3\text{CH}_4 + a_4\text{C}_2\text{H}_6 + a_5\text{C}_6\text{H}_6 + a_6\text{H}_2 + a_7\text{H}_2\text{O} + a_8\text{N}_2 + a_9\text{H}_2\text{S} \tag{R1}$$

2.3. Heterogeneous Reactions. Char−gas reactions are heterogeneous; therefore, corresponding correlations that can reflect the particle reaction characteristics should be developed. During the past few years, many mathematical models have been developed by investigators to model the particle heterogeneous reaction process, such as the fixed-core model (FCM),[32] the shrinking-core model (SCM),[14] the fractal dimension model (FDM),[33] and the random pore model (RPM).[34] Among those models, the shrinking-core model (SCM) is most widely used and can be written as eq 4[14,15]

$$R_s = \frac{(p - p^*)}{\frac{1}{k_{diff}} + \frac{1}{k_{dash}}\left(\frac{1-Y}{Y}\right) + \frac{1}{Y^2 k_s}} \tag{4}$$

where R_s is the reaction rate in g cm^{-2} s^{-1}, $p - p^*$ is the effective partial pressure in atm, K_{diff} is the gas film diffusion constant, K_{dash} is

dx.doi.org/10.1021/ef401302b | Energy Fuels 2013, 27, 6388−6396

Table 1. Kinetic Correlations for the Homogeneous Reactions

reaction	kinetic correlation	reference
$CO + H_2O \rightarrow CO_2 + H_2$ (R2)	$R_2 = k_{21}\left(\frac{p_{CO}}{RT}\right)\left(\frac{p_{H_2O}}{RT}\right) - k_{22}\left(\frac{p_{CO_2}}{RT}\right)\left(\frac{p_{H_2}}{RT}\right)$	
	$k_{21} = 2.75 \times 10^3 \exp(-8.36 \times 10^4/(RT))$	26
	$K_{eq2} = 2.65 \times 10^{-2} \exp(3956/T)$	27
	$k_{22} = k_{21}/K_{eq2}$	
$CH_4 + H_2O(g) \rightarrow CO + 3H_2$ (R3)	$R_3 = k_{31}\left(\frac{p_{CH_4}}{RT}\right)\left(\frac{p_{H_2O}}{RT}\right) - k_{32}\left(\frac{p_{CO}}{RT}\right)\left(\frac{p_{H_2}}{RT}\right)^3$	
	$k_{31} = 312 \exp(-1.67 \times 10^5/RT)$	28
	$K_{eq3} = 6.7125 \times 10^{-24} \exp(27020/T) \times (RT)^2$	27
	$k_{32} = k_{31}/K_{eq3}$	
$C_6H_6 + 6H_2O(g) \rightarrow 6CO + 9H_2$ (R4)	$R_4 = k_4\left(\frac{p_{C_6H_6}}{RT}\right)\left(\frac{p_{H_2O}}{RT}\right) \times 1000$	29
	$k_4 = 312 \exp(-1.256 \times 10^5/RT)$	
$C_6H_6 + 8H_2 \rightarrow 4CH_4 + C_2H_6$ (R5)	$R_5 = 1.7 \times 10^4 \exp(98409.38/RT)\varepsilon_0\rho_g y_{tar}/M_{tar}$	
	$\varepsilon_0 = 0.3$	30
	$\rho_g = \frac{p_t}{RT}\left(\sum_{j=1}^{9} y_j/M_j\right)^{-1}$	
$C_2H_6 + 2H_2O(g) \rightarrow 2CO + 5H_2$ (R6)	$R_6 = k_6 n_{C_2H_6}$	
	$k_6 = 312 \exp(-30000/1.987T)$	31

the ash film diffusion constant and can be calculated from eq 6, Y is the parameter reflecting the thickness of the ash layer and can be calculated from eq 5, and k_s is the surface reaction rate constant

$$Y = [(1 - x_{coal})/(1 - f)]^{1/3} \quad (5)$$

where x_{coal} is the coal conversion fraction based on original dry coal at any time after pyrolysis is completed and f is the coal conversion fraction based on original dry coal when pyrolysis is finished

$$k_{dash} = k_{diff}(\varepsilon_a^{2.5}) \quad (6)$$

where ε_a is the voidage in the ash layer and is assumed to be a constant value of 0.75 or 0.5, as reported.[14,15] In this work, the value of 0.75 is assigned to ε_a.

As is known, the heterogeneous reaction rate is related to the char reactive surface area (CRSA). Therefore, a reasonable prediction of CRSA is required for this model. SCM considers the particle grains as idealized balls, and the reactive surface area is the outer surface area of the ball. However, this is not the truth in practice. The actual coal particles are porous grains, and the reactions usually take place on the inner surface of the pores. RPM can reasonably reflect this character and the pore diffusion, but the gas film and ash layer diffusion actions are not taken into account.[34] In this work, SCM and RPM are combined together to model the char gasification process. The kinetics of reaction and diffusion are calculated with the SCM, while the evolution of the particle reactive surface is calculated with the RPM. The evolution of the internal surface area during char conversion is expressed as eq 7

$$\frac{S}{S_0} = (1 - x_{char})\sqrt{1 - \psi \ln(1 - x_{char})} \quad (7)$$

where S_0 denotes the initial internal reactive area, S denotes the reactive area at any time during the reaction, x_{char} denotes the conversion fraction of char, and ψ is the structure parameter for a particular char particle and can be calculated with eq 8

$$\psi = 4\pi L_0(1 - \varepsilon_0)/S_0^2 \quad (8)$$

where L_0 is the initial total length of the pores and ε_0 is the initial porosity of char. The geometric parameters of the pores can be estimated with the following two equations based on the assumption that the pores are cylindrical and of uniform radius, r_p, if any two of the four parameters (S_0, r_p, L_0, and ε_0) are given.[34,35]

$$S_0 = 2\pi r_p L_0(1 - r_p\sqrt{\pi L_0/3}) \quad (9)$$

$$\varepsilon_0 = \pi r_p^2 L_0\left(1 - 2\frac{r_p}{3}\sqrt{\pi L_0/3}\right) \quad (10)$$

It is quite evident, from eq 7, that the calculation of S_0 is very important. Some work have been performed by researchers to define S_0, but usually their results are quite different because S_0 depends upon many conditions, such as properties of the parent coal, the pyrolysis conditions, and the absorbate used to measure it.[36] In this work, the initial char surface area, S_0, is considered to be related to the mass ratio of volatile to carbon on a dry and ash-free basis, as indicated in eq 11.[37] A similar correlation can be found in the literature.[35] The correlation indicates that char obtained from low-rank coal with a high volatile content has a high surface area, which is justified

$$S_0 = \frac{227.75}{FC/VM} + 116.31 \quad (11)$$

where FC denotes the fixed carbon mass fraction on the dry and ash-free basis and VM denotes the volatile mass fraction on the dry and ash-free basis.

Three typical heterogeneous reactions, R7−R9, are considered, and the corresponding kinetic correlations are listed in Table 2.

$$C(s) + H_2O \rightarrow CO + H_2 \quad (R7)$$

$$C(s) + 2H_2 \rightarrow CH_4 \quad (R8)$$

$$C(s) + CO_2 \rightarrow 2CO \quad (R9)$$

dx.doi.org/10.1021/ef401302b | Energy Fuels 2013, 27, 6388−6396

Table 2. Kinetic Correlations for the Heterogeneous Reactions[14,15]

kinetic parameters for R7	kinetic parameters for R8	kinetic parameters for R9
$k_s = 1.4505 \times 10^{-2} \exp(-21060/T)$	$k_s = 2.2531 \times 10^{-4} \exp(-17921/T)$	$k_s = 1.0335 \times 10^{-2} \exp(-21060/T)$
$k_{diff} = 5.8734 \times 10^{-8}\left(\frac{T}{2000}\right)^{0.75}/(p_t d_p)$	$k_{diff} = 2.5039 \times 10^{-6}\left(\frac{T}{2000}\right)^{0.75}/(p_t d_p)$	$k_{diff} = 3.117 \times 10^{-8}\left(\frac{T}{2000}\right)^{0.75}/(p_t d_p)$
$K_{eq} = \exp[17.644 - 30260/(1.8T)]$	$K_{eq} = \frac{0.175}{34713}\exp[18400/(1.8T)]$	$p_i - p_i^* = p_{CO_2}$
$p_i - p_i^* = p_{H_2O} - \frac{p_{H_2}p_{CO}}{K_{eq}}$	$p_i - p_i^* = p_{H_2} - \sqrt{p_{CH_4}/K_{eq}}$	

It should be noted that the original kinetic parameters reported in the literature[14,15] are based on the SCM. In the SCM, the particle surface area is considered as the ball outer surface area and the evolution of the surface area is related to the ball volume. In the present work, however, the initial char surface area is calculated with eq 11 and the surface area evolution is based on the RPM, as calculated with eq 7. Therefore, the kinetic parameters need to be recalculated mainly on the basis of the initial surface area of the two models. Moreover, although the effects of species partial pressures on the heterogeneous reaction rates have been reflected with the effective partial pressures, $p - p^*$, the effect of the pyrolysis pressure on the char reactivity is not reflected with eq 4. The char reactivity was found decreasing slowly with the increment of the pyrolysis pressure.[38−41] This is mainly due to two aspects. One is the effect of the pyrolysis pressure on the char surface area, and the other is the effect of the pyrolysis pressure on the char intrinsic reactivity. To identify the effect of the pyrolysis pressure on the char reactivity, a new modified equation, eq 12, is proposed in this work. In this equation, the effect of the pressure on the char reactivity is reflected with a pressure correction item by imitating the temperature correction item in the Arrhenius equation

$$R_s = \frac{(p - p^*)}{\frac{1}{k_{diff}} + \frac{1}{k_{dash}}\left(\frac{1-Y}{Y}\right) + \frac{1}{Y^2 k_s}}\left(\frac{p}{p_r}\right)^n \tag{12}$$

where p_r denotes the reference pressure and n is the pressure exponent. The reference pressure in this work is set as 1000 psi (6 894 757.3 Pa), and it is found that the pressure exponent of −0.070 39 can reasonably reflect the pressure effect on the char reactivity during our calculation.

The model for the heterogeneous reactions proposed in this work, including eqs 5−12, combines the RPM and the SCM and accounts for the effect of the pyrolysis pressure on the char apparent reactivity by pressure correction. Thus, this char−gas heterogeneous model is called the CRPSC−PC model. It is part of the CHG model and specially used to calculate the apparent reaction rates of the char−gas heterogeneous reactions.

3. CFD MODELS

The hydrogasification kinetic model is programmed and loaded to Fluent, via UDF, to model the real gasification process in an entrained-flow-bed coal hydrogasifier. The discrete particle model (DPM) is introduced to model the gas−solid flow with chemical reactions. The fluid phase is treated as a continuum by solving the time-averaged Navier−Stokes equations in the Eulerian coordinate, while the dispersed phase is solved by tracking a large number of particles through the calculated flow field in the Lagrangian coordinate. The dispersed phase can exchange momentum, mass, and energy with the fluid phase.

3.1. Continuous Phase Equations. The general conservation equation form of the reaction flow for the continuous phase can be written as eq 13

$$\frac{\partial \rho\phi}{\partial t} + \nabla(\rho\vec{V}\phi) = \nabla(\Gamma_\phi \nabla\phi) + S_\phi + S_{P\phi} \tag{13}$$

where ρ, t, ϕ, $\vec{V}$, Γ_ϕ, S_ϕ and $S_{P\phi}$ are the fluid density, time, general scalar, velocity vector, effective diffusivity, gas-phase source term, and particle source term, respectively.[42] An equation set of steady-state conservation equations can be used to describe the gas-phase reaction flow, including mass, momentum, enthalpy, species mass fraction, turbulence kinetic energy, and its rate of dissipation. The standard $k-\varepsilon$ (SKE) model is used to calculate the turbulence in the hydrogasifier, where no swirl velocity or counter flow occurs. Detailed description about the SKE model can be found in the literature.[43]

The eddy-dissipation concept (EDC) is used to calculate the turbulent reaction.[44] It assumes that the reaction occurs in small turbulent structures, called the fine scales. The length fraction of the fine scales is modeled as eq 14[45]

$$\xi^* = C_\xi\left(\frac{\nu\varepsilon}{k^2}\right)^{1/4} \tag{14}$$

where ξ^* denotes fine-scale quantities, C_ξ is the volume fraction constant that equals 2.1377, and ν is the kinematic viscosity. The volume fraction of the fine scales is calculated as ξ^{*3}. Species are assumed to react in the fine structures over a time scale τ^* as given by eq 15

$$\tau^* = C_\tau\left(\frac{\nu}{\varepsilon}\right)^{1/2} \tag{15}$$

where C_τ is a time scale constant equal to 0.4082.

3.2. Discrete Phase Equations. The particle trajectory is calculated by integrating the force balance equation written in a Lagrangian reference frame as eq 16

$$\frac{du_p}{dt} = F_D(u - u_p) + \frac{g(\rho_p - \rho)}{\rho_p} + F \tag{16}$$

where F is an additional acceleration term, g is the gravitational acceleration, $F_D(u - u_p)$ is the drag force per unit particle mass and F_D can be calculated with eq 17, u is the fluid-phase velocity, u_p is the particle velocity, ρ is the fluid density, and ρ_p is the particle density

$$F_D = \frac{18\mu}{\rho_p d_p^2}\frac{C_D Re}{24} \tag{17}$$

where μ is the molecular viscosity, d_p is the particle diameter, and Re is the relative Reynolds number and is defined by eq 18.

$$Re = \frac{\rho d_p |u_p - u|}{\mu} \tag{18}$$

dx.doi.org/10.1021/ef401302b | Energy Fuels 2013, 27, 6388−6396

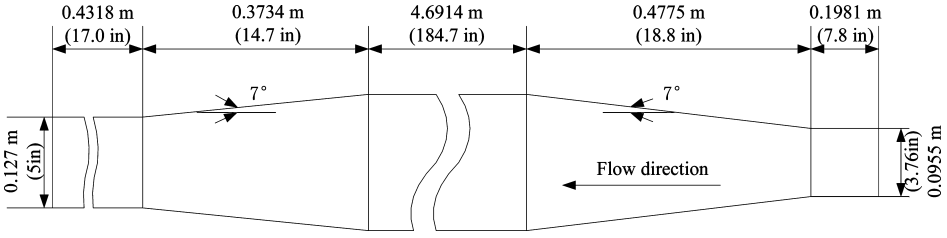

Figure 2. Schematic diagram of the hydrogasifier used in experiments 1−5.[11]

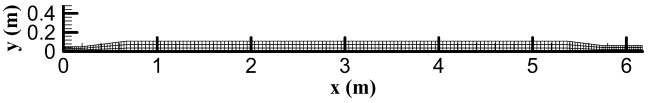

Figure 3. Mesh for the axisymmetric hydrogasifier.

The net rate of the coal particle mass consumption is the sum of all particle reaction rates. If one species in the continuous phase is consumed in the particle reaction, a negative source will be supplied during the computation of the species transport equation for this species or else a positive source will be supplied.

The momentum transfer from the continuous phase to the discrete phase is calculated with eq 19 in Fluent

$$\text{momentum} = \sum (F_D(u - u_p) + F_{other})\dot{m}_p \Delta t \tag{19}$$

where $\dot{m}_p$ is the particle mass flow rate, F_{other} denotes other interaction forces per unit particle mass, and Δt is the time step.

The heat transfer from the continuous phase to the discrete phase is calculated with eq 20 in Fluent[42]

$$m_p c_p \frac{dT_p}{dt} = hA_p(T_\infty - T_p) - f_h \frac{dm_p}{dt} H_{reac} + A_p \varepsilon_p \sigma(\theta_R{}^4 - T_p{}^4) \tag{20}$$

where h is the convection heat transfer coefficient, A_p denotes the particle heat exchange area, T_∞ denotes the local temperature of the continuous phase, T_p is the particle temperature, H_{reac} is the heat formation of the surface reaction, f_h is the percentage of H_{reac} absorbed by the particle, ε_p is the particle emissivity, σ is the Stefan−Boltzmann constant, and θ_R is the radiation temperature.

3.3. Radiative Heat Transfer Model. Five radiation models, including the discrete transfer radiation model (DTRM),[46,47] the P-1 radiation model,[48] the Rosseland radiation model,[49] the surface-to-surface (S2S) radiation model,[50] and the discrete ordinates (DO) radiation model,[49] are provided by Fluent. Thereinto, only the P-1 and DO radiation models allow for the particle radiation. The P-1 radiation model is justified when the optical thickness defined by eq 21 is larger than 1, while the DO radiation model can be used in a wide range of optical thicknesses. In this work, the optical thickness is relatively small (less than 1); therefore, the DO radiation model is chosen to model the radiative heat transfer. The weighted-sum-of-gray-gases model (WSGGM)[51] is used to calculate the adsorption coefficient of the gaseous mixture. The emissivity of the inner wall and particle are set to 0.85 and 0.9, respectively

$$\tau = (\alpha + \sigma_s)s \tag{21}$$

where α is the absorption coefficient, σ_s is the scattering coefficient, and s is the characteristic length.

3.4. Summary of the Simulation Procedure. To make it clearer, the simulation procedure is summarized in this section. It should be noticed that the flow in the simulation is a gas−solid two-phase flow with chemical reactions. The continuous phase is modeled in the Eulerian coordinate, while the dispersed phase is modeled in the Lagrangian coordinate. The SKE model is used to model the turbulence in the flow, and the turbulent chemical reactions are modeled using the EDC method. The whole reactions in the simulation are modeled using the CHG model set up in this work. The evolution of the particle mass, momentum, and energy are modeled with the DPM method. Two-way coupling between the particle and the fluid is chosen so that the effects of the solid phase on the continuous phase are considered by the source terms in the continuous phase governing equations. Radiation heat transfer in the simulation is taken into account and modeled with the DO radiation model. In this work, the convection term of the governing equations are discretized using the second-order upwind scheme and the whole equation set is solved using the SIMPLE algorithm.

4. MODEL VALIDATION

To evaluate the reliability and accuracy of the CHG kinetic model set up in this work, in total, seven sets of experimental data obtained from different cylindrical entrained-flow coal hydrogasifiers in the Rockwell reports[11,12] are used to do the model validation. The overall object of the experiments in the Rockwell reports was to generate data required to verify the corresponding chemical reaction mechanisms. The geometry parameters of the reactor and the boundary conditions (BCs) were all given clearly in those reports so that they are proper to be used to do the model validation.

4.1. Case Description. In the experiments reported in ref 11, experiments 1−5, the whole gasification equipment was divided

Table 3. Analyses of Coal Used in the Experiments and Numerical Cases

	approximate analysis				ultimate analysis				
	M_{ar}	A_{ar}	C_{ar}	V_{ar}	C	H	O	N	S
experiments 1−5/cases 1−5	1.95	8.27	50.66	39.11	81.39	5.60	8.04	1.64	3.32
experiment 6/case 6	5.52	8.37	49.92	36.19	80.35	5.56	9.89	1.16	3.04
experiment 7/case 7	9.40	16.87	19.97	53.76	46.84	4.97	27.57	1.25	2.03

dx.doi.org/10.1021/ef401302b | Energy Fuels 2013, 27, 6388−6396

into four parts, including the preburner, where the fast reaction of oxygen and excessive hydrogen took place, the steam generator, where water and additional hydrogen were injected, the main burner, where additional oxygen was injected and reacted with excessive hydrogen, and the hydrogasifier, where coal was injected along with nitrogen and the CHG took place. Reaction in the first three parts, the preburner, the steam generator, and the main burner, is the fast combustion of hydrogen, which prepares the hydrogasification agent (surplus hydrogen and water) required. In the fourth part, hydrogasifier, the gasification agent mixes and reacts with the feed coal. Namely, the CHG process actually took place in the hydrogasifier. A two-dimensional (2D) axisymmetric object is used to model the reactor in the cylindrical coordinate. The schematic diagram of the hydrogasifier is shown in Figure 2, and the symmetric axis is set along the x direction. Before the numerical simulation, three levels of grids with different numbers of quadrangular cells are tested to obtain the mesh-independent results, and the final mesh is shown in Figure 3. In the experiments reported in ref 12, experiments 6 and 7, two different cylindrical entrained flow reactors are used. The inner diameter and length of the reactor in experiment 6 are 4.87 in (0.124 m) and 10 ft (3.048 m), respectively. The inner diameter and length of the reactor in experiment 7 are 4.26 in (0.108 m) and 15 ft (4.572 m), respectively. The geometric configuration and mesh of these two reactors are relatively simple, and they are not shown in this paper. The mesh sensitivity analyses of all the cases have been done and finally a set of meshes with proper amount of nodes are chosen to get the mesh independent results. The proximate and ultimate analyses of the pulverized coal used in those experiments are listed in Table 3. The BCs of the seven experiments and the corresponding numerical cases are listed in Table 4.

4.2. Model Validation. The SIMPLE method is used to solve the numerical equation sets, and the second-order upwind scheme is chosen to discrete the convection term of the governing equations. The iteration residuals and the outlet area-weighted-average methane mole fraction are observed to decide whether the calculation is converged or not. After convergence, residuals of the continuity (pressure correction), turbulence, and species mass fraction equations have all reached the order of 10^{-4}; residuals of energy and radiation equations have reached the order of 10^{-6}; and the outlet methane mole fraction has basically reached a constant number. The comparisons of the numerically calculated and the experimental mole fractions (%) of the species in the hydrogasification products are listed in Table 5.

The square sum of errors, error, defined by eq 22[27,28] and listed in Table 5, is used to evaluate the reliability and accuracy of the CRPSC−PC model set up in this work

$$\text{error} = \sum_{i=1}^{I} (Y_i^{\text{C}} - Y_i^{\text{E}})^2 \tag{22}$$

where I is the total number of constituent species in the gasification product and Y_i^{C} and Y_i^{E} are the calculated and experimental mole fractions of species i, respectively. It can be seen from Table 5 that the simulation results agree well with the experimental data, except for the mole fractions of CO and CO_2, especially when their values are small. This is because, in the experiments, the initial gasification agents are actually H_2 and O_2. However, in the simulation of this work, H_2 and O_2 are supposed to be ideally mixed and all of the oxygen has been

Table 4. BCs of the Experiments and Numerical Cases

BCs	experiment 1/case 1	experiment 2/case 2	experiment 3/case 3	experiment 4/case 4	experiment 5/case 5	experiment 6/case 6	experiment 7/case 7
H_2 flow rate (lbs/h)	347	344.625	216.25	287.125	244	225.86	199.49
H_2O flow rate (lbs/h)	486	516.375	1664.75	1038.875	1507	95.99	135.68
N_2 flow rate (lbs/h)	97.33	100.59	97.02	103.63	98.28	96.67	55.80
coal flow rate (lbs/h)	927	958	924	987	936	579.24	254.88
inlet temperature (K)	1355	1400	1531	1470	1351	1301	1387.04
pressure (psi)	1015	1015	1015	1014	1013	1492	503

dx.doi.org/10.1021/ef401302b | Energy Fuels 2013, 27, 6388−6396

Table 5. Comparisons of the Outlet Species Mole Fractions

experiments	species	H_2	CH_4	H_2O	CO	CO_2	N_2	H_2S	error
experiment 1	experiment[11]	69.593	11.904	14.877	0.874	0.107	1.915	0.347	0.7688
	case 1	69.039	12.161	15.164	0.521	0.540	1.951	0.354	
experiment 2	experiment[11]	65.141	15.573	15.017	1.716	0.153	1.996	0.372	0.7818
	case 2	64.275	15.700	15.074	1.615	0.159	2.043	0.369	
experiment 3	experiment[11]	40.782	12.217	39.841	3.487	1.464	1.815	0.364	1.6227
	case 3	40.188	12.562	38.873	3.782	1.814	1.863	0.319	
experiment 4	Exp.[11]	52.351	14.718	27.372	2.539	0.58	2.024	0.387	1.9177
	case 4	51.175	15.367	27.058	2.634	0.638	2.067	0.360	
experiment 5	experiment[11]	44.583	10.354	40.924	1.015	0.351	1.825	0.338	5.2492
	case 5	45.432	10.699	38.900	1.449	0.700	1.871	0.316	
experiment 6	experiment[12]	78.55	16.55		1.29	0.12	3.48		1.2721
	case 6	77.61	17.05		0.96	0.02	3.34		
experiment 7	experiment[12]	91.70	3.74		2.37	0.11	2.08		1.0488
	case 7	92.25	3.67		1.51	0.08	2.05		

Table 6. Comparisons of the Gas Outlet Temperatures

	experiment 1	experiment 2	experiment 3	experiment 4	experiment 5	experiment 6	experiment 7
experiments[11,12]	1280	1356	1339	1351	1240		
calculated results	1308	1372	1327	1348	1262	1485	1359

Table 7. Comparisons of the Particle Residence Times

	experiment 1	experiment 2	experiment 3	experiment 4	experiment 5	experiment 6	experiment 7
experiments[11,12]	5.4	5.1	4.8	5.0	5.3	2.290	1.075
calculated results	5.39	5.03	4.99	5.05	5.50	2.286	0.966

converted into H_2O at the inlet of the hydrogasifier because the amount of H_2 is relatively excessive. Therefore, the reaction of residual O_2 and carbon in the hydrogasifier are not considered. Although there are deviations between the experimental value and the calculated results of the mole fraction of CO and CO_2, it does not matter for the CHG process because CO and CO_2 are not the staples and the yields of them are very little.

In the CHG process, the reaction temperature and the particle residence time are of great importance because they closely related to the chemical reaction extent and the char conversion ratio. The comparisons of the outlet gas temperature (K) between the experimental data and the numerical results are listed in Table 6. It can be seen that the calculated temperatures are very close to those from the experiments, and the relative errors are around 2%. Temperatures of experiments 6 and 7 are not given because there is a quench equipment assembled at the outlet of the reactor and it has a significant effect on the outlet gas temperature.[12] In fact, the reaction temperature is coupled with the extent of the CHG process. Different stages of the CHG process correspond to different compositions of the product. The difference of the total formation heats between the species of one CHG stage and the initial stage decides the net heat generated and, consequently, decides the temperature of this stage. Therefore, with the given BCs, if the calculated outlet product composition is close to the experimental outlet product composition, the calculated temperature should be close that from the experiment. The comparison of the particle residence time (s) between the experiments and the numerically calculated results is shown in Table 7. Because the particle is injected straightly along the axis and no swirl occurs, the particle trajectory is simple and close to a straight line. In this case, the 2D numerical simulation can well reflect the actual particle residence time. The comparisons indicate that the particle residence time predicted with the DPM used in this work agrees very well with the experimental data, which confirms that the DPM is justified to be able to model the particle movements in the entrained-flow-bed reactor.

5. ANALYSES OF THE CHG PROPERTIES

To find out the CHG properties in the cylindrical reactors, the experiments reported in the literature[11,12] rather than the simulation predictions are analyzed because the experiments have fully reflected the hydrogasification characteristics. Comparisons of experiments 1 and 5, which have similar gasification conditions, except for the composition of the gasification agent, indicate that increasing the H_2O concentration in the gasification agent can increase the CH_4 concentration in the dry gasification product. For example, the mole fraction of CH_4 is 13.98 in experiment 1, while it is 17.52 in experiment 5 in the dry base product. This is because the reaction rate of R8 is relatively higher than that of R7. R8 is, however, an endothermic reaction; therefore, additional heat energy will be consumed if the H_2O concentration is high, and it is adverse to the gasification efficiency. Comparisons of experiments 3 and 5, which have similar gasification conditions, except for the inlet gas temperature, indicate that increasing the inlet gas temperature can increase the CH_4 concentration in the gasification product when the H_2O concentration of the gasification agent is high. This is also because R8 is an endothermic reaction. The mole fraction of CH_4 in the gasification product in experiment 6 is much higher than that in experiment 7, which indicates that an increasing reaction pressure can greatly promote the hydrogasification process when the H_2 concentration in the gasification agent is high. This is because R7 can reduce the total gaseous species in the gasifier and an increasing pressure will extend the char hydrogenation reaction. Through these comparisons, it can be seen that an increasing H_2O concentration can

dx.doi.org/10.1021/ef401302b | Energy Fuels 2013, 27, 6388−6396

increase the CH_4 concentration in the dry gasification product, an increasing temperature can increase the CH_4 concentration in the gasification product when the concentration of H_2O in the gasification agent is high, and an increasing pressure can obviously increase CH_4 in the gasification agent when the H_2 concentration of the gasification agent is high.

6. CONCLUSION

A CHG kinetic model, including five homogeneous reactions and three heterogeneous reactions, is established in this work. To make the simulation of heterogeneous reactions become closer to the actual process, a CRPSC−PC model, which integrates the advantages of the SCM and RPM and allows for the effect of the pyrolysis pressure on the char reactivity, is developed to calculate the char−gas heterogeneous reaction rates. The gasification model is then loaded to Fluent, via UDF, and validated against the experimental data. Then, the CHG properties in the cylindrical gasifiers are analyzed on the basis of the reported experimental data. From the study in this work, the following conclusions can be drawn: (1) The hydrogasification model can accurately predict the product species composition of the entrained-flow CHG. Therefore, it can be definitely used to predict the effects of different operating parameters on entrained-flow CHG. (2) The CRPSC−PC model is presented to deal with the effect of the pyrolysis pressure on the char reactivity and is justified to be capable of predicting the char heterogeneous reactions. (3) The EDC model is reasonable to calculate the hydrogasification reactions in turbulent flow, and the DPM can be used to properly predict the particle movement in the entrained-flow coal hydrogasifier. (4) The concentration of CH_4 in the gasification product can be increased by increasing the H_2O concentration in the gasification agent, increasing the inlet temperature of the gasification agent when the H_2O concentration is high, and increasing the gasification pressure when the H_2 concentration is high.

AUTHOR INFORMATION

Corresponding Author

*Telephone: +86-10-5168-8542. Fax: +86-10-5168-8404. E-mail: hebs@bjtu.edu.cn.

Notes

The authors declare no competing financial interest.

ACKNOWLEDGMENTS

The authors gratefully acknowledge financial support from the National Natural Science Foundation of China (NSFC, 50876008 and 51176009) and the Fundamental Research Funds for the Central Universities (2013YJS078) for this work.

NOMENCLATURE

BC = boundary condition
CFD = computational fluid dynamics
CRPSC−PC = combined random pore and shrinking-core model with pressure correction
CRSA = char-reactive surface area
DO = discrete ordinates
DPM = discrete particle model
DTRM = discrete transfer radiation model
EDC = eddy-dissipation concept
FCM = fixed-core model
FDM = fractal dimension model
IGT = Institute of Gas Technology
LANL = Los Alamos National Laboratory
RPM = random pore model
S2S = surface-to-surface
SCM = shrinking-core model
SKE = standard $k-\varepsilon$
UDF = user-defined function
WSGGM = weighted-sum-of-gray-gases model
ZEC = zero emission coal
ZECA = Zero Emission Coal Alliance

REFERENCES

(1) Energy Information Administration (EIA). *International Energy Outlook 2011*; EIA: Washington, D.C., 2011; Contract DOE/EIA-0484(2011), http://me.queensu.ca/Courses/430/InternationalEnergyOutlook-summaryonly.pdf.

(2) Gao, L.; Paterson, N.; Fennell, P.; Dugwell, D.; Kandiyoti, R. The zero emission carbon concept (ZECA): Extents of reaction with different coals in steam/hydrogen, tar formation and residual char reactivity. *Energy Fuels* **2008**, *22* (4), 2504−2511.

(3) Ziock, H.-J.; Lackner, K. S.; Harrison, D. P. *Zero Emission Coal Power, A New Concept*; Los Alamos National Laboratory: Los Alamos, NM, 2001; Contract LA-UR-01-2214, http://www.netl.doe.gov/publications/proceedings/01/carbon_seq/2b2.pdf.

(4) He, B. S.; Li, M. Y.; Wang, X.; Zhu, L.; Wang, L. L.; Xue, J. W.; Chen, Z. X. Chemical kinetics-based analysis for utilities of ZEC power generation system. *Int. J. Hydrogen Energy* **2008**, *33*, 4673−4680.

(5) Yan, L. B.; He, B. S.; Ma, L. L.; Pei, X. H.; Wang, C. J.; Li, X. S. Integrated characteristics and performance of zero emission coal system. *Int. J. Hydrogen Energy* **2012**, *37*, 9669−9676.

(6) Yan, L. B.; He, B. S.; Pei, X. H.; Li, X. S.; Wang, C. J.; Liang, H. X. Kinetic model and prediction for coal hydrogasification. *Int. J. Hydrogen Energy* **2013**, *38* (11), 4513−4523.

(7) Steinberg, M. *Process for Conversion of Coal to Substitute Natural Gas (SNG)*; HCE LLC: New York, 2005; Contract HCEI-8-05-001r2, http://www.hceco.com/HCEI805001.pdf.

(8) Tang, L. H.; Zhu, Z. B.; Gu, H. X.; Zhang, C. F. The effect of coal rank on flash hydropyrolysis of Chinese coal. *Fuel Process. Technol.* **1999**, *60*, 195−202.

(9) Porada, S. A comparison of basket willow and coal hydrogasification and pyrolysis. *Fuel Process. Technol.* **2009**, *90*, 717−721.

(10) Zhang, A.; Kaiho, M.; Yasuda, H.; Zabat, M.; Nakano, K.; Yamada, O. Fundamental studies on hydrogasification of Taiheiyou coal. *Energy* **2005**, *30*, 2243−2250.

(11) Falk, A. Y.; Schuman, M. D.; Kahn, D. R. *Advancement of Flash Hydrogasification: Task VIII—Performance Testing*; Morgantown Energy Technology Center: Morgantown, WV, 1986; Contract DE-AC21-78ET10328, http://www.osti.gov/bridge/purl.cover.jsp?purl=/5377768 -SKAxm4/5377768.pdf.

(12) Friedman, J. *Development of a Single-Stage, Entrained-Flow, Short-Residence-Time Hydrogasifier*; National Technical Information Service: Alexandria, VA, 1979; Contract FE-2518-24.

(13) Epstein, M.; Chen, T. P.; Ghaly, M. A. *An Analysis of Coal Hydrogasification Process*; Energy Research and Development Administration: Washington, D.C., 1977; Contract EF-77-A-01-2565, www.osti.gov/bridge/servlets/purl/6074682-KtEPFx/6074682.pdf.

(14) Wen, C. Y.; Chaung, T. Z. Entrainment coal gasification modelling. *Ind. Eng. Chem. Proc. Des. Dev.* **1979**, *18*, 684−694.

(15) Liu, X. J.; Zhang, W. R.; Park, T. J. Modelling coal gasification in an entrained flow gasifier. *Combust. Theor. Model.* **2001**, *5*, 595−608.

(16) Blackwood, J. D. The kinetics of the system carbon−hydrogen−methane. *Aust. J. Chem.* **1962**, *15*, 397−408.

(17) Blackwood, J. D.; McCarthy, D. J. The mechanism of hydrogenation of coal to methane. *Aust. J. Chem.* **1966**, *19*, 797−813.

(18) Wen, C. Y.; Heubler, J. kinetic study of coal char hydrogasification. Rapid initial reaction. *Ind. Eng. Chem. Proc. Des. Dev.* **1965**, *4*, 147−154.

(19) Anthony, D. B.; Howard, J. B. Coal devolatilization and hydrogasification. *AIChE J.* **1976**, *22*, 625−656.
(20) Moseley, F.; Paterson, D. The rapid high temperature hydrogenation of coal chars. Part 1: Hydrogen pressures up to 100 atm. *J. Inst. Fuel* **1965**, *288*, 13−23.
(21) Tomerczek, J.; Gil, S. The kinetics of coal chars hydrogasification. *Fuel Process. Technol.* **2010**, *91*, 1564−1568.
(22) Hippo, E. J.; Johnson, J. L. *Modeling of Initial Stage Hydrogasification of Various Ranked Coals*; Institute of Gas Technology: Chicago, IL, 1978; Report CONF7809025, http://www.osti.gov/bridge/purl.cover.jsp?purl=/6074682-KtEPFx/6074682.pdf.
(23) Johnson, J. L. *Kinetics of Initial Coal Hydrogasification Stages*; Institute of Gas Technology: Chicago, IL, 1977; Report CONF770301P2, http://web.anl.gov/PCS/acsfuel/preprint%20archive/Files/22_2_NEW%20ORLEANS_03-77_0017.pdf.
(24) Kobayashi, H.; Howard, J. B.; Sarofim, A. F. Coal devolatilization at high temperatures. *Symp. (Int.) Combust., [Proc.]* **1977**, 411−425.
(25) Wang, T.; Silaen, A. Effects of turbulence and devolatilization models on gasification simulation. *Proceedings of the 25th Annual International Pittsburgh Coal Conference*; Pittsburgh, PA, Sept 29−Oct 2, 2008.
(26) Wu, Y. X.; Zhang, J. S.; Yue, G. X.; Lv, J. F. Analysis of dominating process between mixing and reactions in a Texaco coal gasifier. *J. Combust. Sci. Technol.* **2009**, *15*, 287−292 , in Chinese.
(27) Watkinson, A. P.; Lucas, J. P.; Lim, C. J. A prediction of performance of commercial coal gasifiers. *Fuel* **1991**, *70*, 519−527.
(28) Wu, X. C.; Wang, Q. H.; Luo, Z. Y.; Fang, M. X.; Cen, K. F. Modelling on effects of operation parameters on entrained flow coal gasification (I): Model established and validation. *J. Zhejiang Univ. (Eng. Sci.)* **2004**, *38*, 1363−1365 , in Chinese.
(29) Kumar, M.; Zhang, C.; Monaghan, R. F. D.; Singer, S. L.; Ghoniem, A. F. CFD simulation of entrained flow gasification with improved devolatilization and char consumption submodels. *IMECE2009: ASME 2009 International Mechanical Engineering Congress and Exposition*; Lake Buena Vista, FL, Nov 13−19, 2009.
(30) Goyal, A. Mathematical modelling of entrained-flow coal gasification reactors. Ph.D. Dissertation, Illinois Institute of Technology, Chicago, IL, 1980.
(31) Li, Z.; Wang, T. J.; Han, Z. M.; Zheng, H. T.; Ni, W. D. Study on mathematical models of Texaco gasifier modelling. *Power Eng.* **2001**, *21*, 1161−1165 , in Chinese.
(32) Brown, B. W.; Smoot, L. D.; Smith, P. J.; Hedman, P. O. Measurement and prediction of entrained-flow gasification processes. *AIChE J.* **1988**, *34*, 435−446.
(33) Borgwart, R. H. Calcination kinetics and surface area of dispersed limestone particles. *AIChE J.* **1985**, *31*, 103−111.
(34) Bhatia, S. K.; Perlmutter, D. D. A random pore model for fluid-solid reactions: 1. Isothermal, kinetic control. *AIChE J.* **1980**, *26*, 379−386.
(35) Liu, G.; Benyon, P.; Benfell, K. E.; Bryant, G. W.; Tate, A. G.; Boyd, R. K.; Harris, D. J.; Wall, T. F. The porous structure of bituminous coal chars and its influence on combustion and gasification under chemically controlled conditions. *Fuel* **2000**, *179*, 617−626.
(36) Liu, G. S.; Rezaei, H. R.; Lucas, J. A.; Harris, D. J.; Wall, T. F. Modelling of a pressurized entrained flow coal gasifier: The effect of reaction kinetics and char structure. *Fuel* **2000**, *79*, 1767−1779.
(37) Hla, S. S.; Harris, D.; Roberts, D. *Gasification Conversion Model-PEFR*; Cooperative Research Centre for Coal in Sustainable Development: Australia, 2008; Research Report 80, http://www.ccsd.biz/publications/files/RR/ACF5066.pdf.
(38) Messenböck, P. C.; Paterson, N. P.; Dugwell, D. R.; Kandiyoti, R. Factors governing reactivity in low temperature coal gasification. Part 1. An attempt to correlate results from a suite of coals with experiments on maceral concentrates. *Fuel* **2000**, *79*, 109−121.
(39) Yang, H. P.; Chen, H. P.; Ju, F. D.; Wang, J.; Zhang, S. H. Study on pressurized pyrolysis and gasification of Chinese typical coal samples. *Proc. CSEE* **2007**, *27*, 18−22 , in Chinese.
(40) Cetin, E.; Gupta, R.; Moghtaderi, B. Effect of pyrolysis pressure and heating rate on radiata pine char structure and apparent gasification reactivity. *Fuel* **2005**, *84*, 1328−1334.
(41) Gadiou, R.; Bouzidi, Y.; Prado, G. The devolatilisation of millimetre sized coal particles at high heating rate: The influence of pressure on the structure and reactivity of the char. *Fuel* **2002**, *81*, 2121−2130.
(42) Fluent, Inc. *FLUENT6.3-User's Guide*; Fluent, Inc.: New York, 2006.
(43) Launder, B. E.; Spalding, D. B. *Lectures in Mathematical Models of Turbulence*; Academic Press: London, U.K., 1972.
(44) Magnussen, B. F. On the structure of turbulence and a generalized eddy dissipation concept for chemical reaction in turbulent flow; *Proceedings of the 19th American Institute of Aeronautics and Astronautics (AIAA) Aerospace Sciences Meeting*; St. Louis, MO, Jan 12−15, 1981; http://folk.ntnu.no/ivarse/edc/EDC1981.pdf.
(45) Gran, I. R.; Magnussen, B. F. A numerical study of a bluff-body stabilized diffusion flame. Part 2. influence of combustion modeling and finite-rate chemistry. *Combust. Sci. Technol.* **1996**, *119*, 191−217.
(46) Carvalho, M. G.; Farias, T.; Fontes, P. Predicting radiative heat transfer in absorbing, emitting, and scattering media using the discrete transfer method. In *Fundamentals of Radiation Heat Transfer*; Fiveland, W. A., Croshie, A. L., Smith, A. M., Smith, T. F., Eds.; American Society of Mechanical Engineers (ASME): New York, 1991; Vol. *160*, pp 17−26.
(47) Shah, N. G. A new method of computation of radiant heat transfer in combustion chambers. Ph.D. Dissertation, Imperial College of Science and Technology, London, U.K., 1979.
(48) Cheng, P. Two-dimensional radiating gas flow by a moment method. *AIAA J.* **1964**, *2*, 1662−1664.
(49) Siegel, R.; Howell, J. R. *Thermal Radiation Heat Transfer*; Hemisphere Publishing Corporation: Washington, D.C., 1992.
(50) Chui, E. H.; Raithby, G. D. Computation of radiant heat transfer on a non-orthogonal mesh using the finite-volume method. *Numer. Heat. Transfer, Part B* **1993**, *23*, 269−288.
(51) Smith, T. F.; Shen, Z. F.; Friedman, J. N. Evaluation of coefficients for the weighted sum of gray gases model. *J. Heat Transfer* **1982**, *104*, 602−608.